Comparison of PIV measurements and CFD simulations of the velocity field over bottom racks

Luis G. Castillo, Juan T. García, José M. Carrillo, Antonio Vigueras-Rodríguez
Civil Engineering Department, Hidr@m I+D+i Group, Universidad Politécnica de Cartagena, Spain

ABSTRACT: In this work, the comparison of the velocity field over a bottom rack system measured by Particle Image Velocimetry (PIV) and simulated with numerical simulations (ANSYS CFX v14.0) is presented. Laboratory measurements are taken in a physical device located in the Laboratory of Hydraulic Engineering of the Universidad Politécnica de Cartagena (Spain). Velocity and pressure coefficients of the energy equation are obtained and used to evaluate the water profile along the racks. Pressure distribution along the flow depth is presented for several distances along the rack. Pressure results are compared with the pressure deviation terms from hydrostatic pressure profile proposed by several authors.

1 INTRODUCTION

Bottom intake systems, made by racks disposed longitudinally to flow and located at streambed, are used to derive flood flows from ephemeral gullies in semi-arid regions. The shape and spacing between the bars that constitute the rack have influence in the derived flow per unit length. Leading, therefore, to different discharge coefficient values (Orth et al., 1954). The intake system is a spatially-varied flow with decreasing discharge, in which the curvature of the water profile and the streamlines creates a non-hydrostatic pressure distribution over the bottom rack. Following previous studies of Mostkow (1957), Righetti and Lanzoni (2008) verified the relation between the angle of streamlines with the plane of the rack and the discharge coefficient. The streamlines slope also influences in the direction of the drag force that water exerts on solids, defining areas of preferential deposition of solids over the racks (Castillo et al., 2013a, 2013b, 2014, 2015).

Several researchers proposed analytical solutions of the continuity and momentum equations in the vertical plane over the rack. Nakagawa (1969) used a a lineal profile for the horizontal velocity component with regard to its average in each section, while Castro-Orgaz and Hager (2011) estimated it as a constant. These solutions provide pressure distribution and its deviation from hydrostatic values.

Mostkow (1957) considered two-dimensional equations of momentum and continuity.

Common solutions to estimate the water profile and the derived flow along bottom intakes consider frictionless irrotational flow with hydrostatic pressure distributions (Garot, 1939; De Marchi, 1947; Noseda, 1956). For the horizontal rack case

$$\frac{dh}{dx} = -2mC_{qh}\frac{\sqrt{h(H-h)}}{2H-3h} \quad (1)$$

where h is the flow depth, H the energy head considered constant, m the void ratio, and C_{qh} the discharge coefficient as a function of the flow depth.

Curvilinear flow over bottom racks and slots have been experimentally characterized in laboratory by several authors using pressure measurements, and obtaining velocity and pressure coefficients (Mostkow, 1957; Nakagawa, 1969; Nasser et al., 1980).

2 OBJETIVES

The definition of velocity and pressure fields along bottom systems and its influence in derived flow are of interest. In this work, a Particle Image Velocimetry (PIV) system is used to define the 2D velocity field in a vertical plane located in the space between bars. Results are compared with computational fluid dynamic (CFD) simulations (ANSYS CFX v14.0).

Velocity and pressure coefficients, α and λ respectively, are defined and used to evaluate the water profile and the derived flow per unit length. For that purpose, the following equation, obtained from frictionless energy equation, has been used:

$$\frac{dh}{dx} = \frac{\frac{d\lambda}{dx}h^2 + \frac{d\alpha}{dx}h(H-\lambda h) - 2C_{qh}m\sqrt{\alpha(H-\lambda h)h}}{\alpha(2H-3\lambda h)} \quad (2)$$

3 MATERIAL AND METHODS

3.1 *Physical device*

An intake system located at the Hydraulic Laboratory of the Universidad Politécnica de Cartagena (Spain) has been used. It consists of a 5.00 m long and 0.50 m wide approximation channel, a rack with different slopes (from horizontal to 33%), a discharge channel, and the channel to collect derived water. Three different racks, with 0.90 m length, are available. All of them are made of aluminium bars with *T* profiles (T 30/25/2 mm). Bars are disposed longitudinally to the inlet flow. The differences between the racks are the spacing between bars, so different void ratios are available (Figure 1).

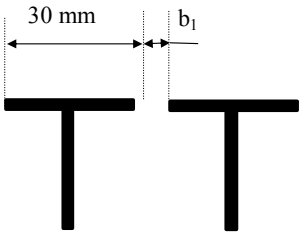

Figure 1. Scheme of bars position

Table 1 summarizes the geometric characteristics of each rack.

Table 1. Geometric characteristic of racks.

Experiment	A	B	C
Spacing between bars, b_1 (mm)	5.70	8.50	11.70
Void ratio $m = \frac{b_1}{b_1 + 30}$	0.16	0.22	0.28

In this work, the rack with void ratio m = 0.28 in the horizontal position was used. Figure 2 shows the intake system in the Hydraulic Laboratory.

3.2 *PIV equipment*

Velocity field was measured with a PIV system composed by a high-speed camera Motion Pro HS-3, 75 mm focal length objective, lens aperture f/11, 520x520 pixel resolution, 8 bits→255 shades and a distance from the camera to stream recorded of 0.50 m. Recording window dimensions are 9x9 cm.

The laser is an Oxford Laser whose configuration is: pulse = 10 μs; beam width = 5.5 mm; power peak = 200 W; delay = 30 μs; wavelength = 808 nm.

The temporal increment between frames is Δt = 1/600 s; so the ratio = 0.00017 meter/pixel. Duration of each test was about 12.5 seconds.

Flow was seeded with polyamide particles of 50 μm size. Frames were analysed in consecutive pairs by cross-correlation in an interrogation area of 64x64 pixel with sub-windows of 32x32 pixel (Thielicke & Stamhuis, 2014).

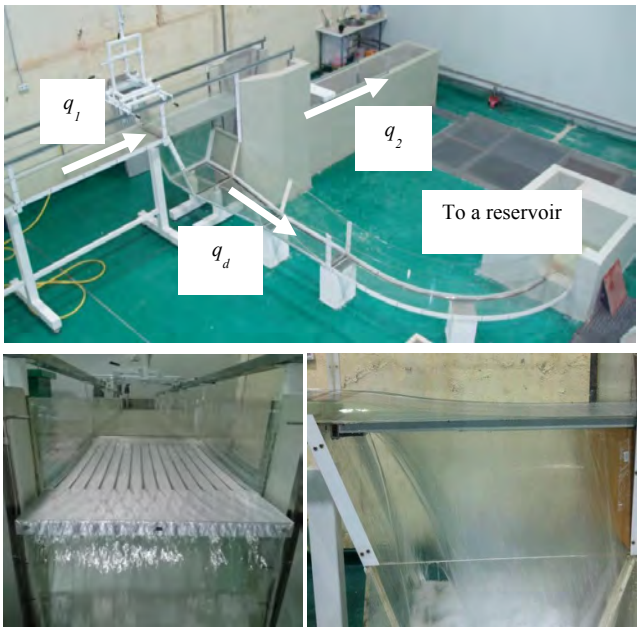

Figure 2. Intake system physical device.

3.3 *Numerical simulations*

A Computational Fluid Dynamics simulation of the intake system with ANSYS CFX v14.0 was also used. Previous works demonstrated the suitability of this code to solve the flow through an intake system (Castillo and Carrillo, 2012; Castillo et al., 2014, 2015).

CFD codes solve the differential Reynolds-Averaged Navier-Stokes (RANS) equations of the phenomenon in the fluid domain, retaining the reference quantity in the three directions for each control volume identified. The equations for conservation of mass and momentum may be written as:

$$\frac{\partial \rho}{\partial t} + \frac{\partial}{\partial x_j}\left(\rho U_j\right) = 0 \quad (3)$$

$$\frac{\partial \rho U_i}{\partial t} + \frac{\partial}{\partial x_j}\left(\rho U_i U_j\right) = -\frac{\partial p}{\partial x_i} + \frac{\partial}{\partial x_j}\left(2\mu S_{ij} - \rho\overline{u_i' u_j'}\right) \quad (4)$$

where i and j are indices, x_i represents the coordinate directions (i, j = 1 to 3 for x, y, z directions, respectively), ρ the flow density, t the time, U the velocity vector, p the pressure, u_i' presents the turbulent velocity in each direction (i = 1 to 3 for x, y, z directions, respectively), μ the molecular viscosity, S_{ij} the

mean strain-rate tensor, and $-\rho\overline{u_i'u_j'}$ the Reynolds stress. Eddy-viscosity turbulence models consider that such turbulence consists of small eddies which are continuously forming and dissipating, and in which the Reynolds stresses are assumed to be proportional to mean velocity gradients. The Reynolds stress may be related to the mean velocity gradients and eddy viscosity by the gradient diffusion hypothesis:

$$-\rho\overline{u_i'u_j'} = \mu_t\left(\frac{\partial U_i}{\partial x_j}+\frac{\partial U_j}{\partial x_i}\right)-\frac{2}{3}\delta_{ij}\left(\rho k+\mu_t\frac{\partial U_k}{\partial x_k}\right) \quad (5)$$

with k being the eddy viscosity or turbulent viscosity, μ_t the eddy viscosity or turbulent viscosity and δ the Kronecker delta function.

The k-ω based Shear-Stress-Transport (SST) turbulence model was selected to complement the numerical solution of the Reynolds-averaged Navier-Stokes equations (RANS). To solve the two-phase air-water, the homogeneous model was used. The fluid domain is divided into control volumes, which must satisfy the balance of the governing equations. The total number of elements used in the simulations was around 350,000 elements, with 0.004 m length scale near the rack.

For simplicity, it was considered that all the longitudinal bars work in the same mode in the intake system. For this reason, the domain fluid considers three bars and two spacing between bars. Symmetry conditions were used in the central plane of the extreme bars.

The model boundary conditions correspond to the flow at the inlet condition (located 0.50 m upstream of the rack), the upstream and downstream water levels and their hydrostatic pressures distributions. In the bottom of the water collected channel, opening boundary condition were used. It has been assumed that the free surface is on the 0.5 air volume fraction. To judge the convergence of iterations in the numerical solution, we monitored the residuals. The solution is said to have converged in the iterations if the scaled residuals are smaller than fixed values ranging between 10^{-3} and 10^{-6}. In this work, the residual values were set to 10^{-4} for all the variables (Castillo et al. 2016).

4 RESULTS

4.1 *Velocity Field*

Particle Image Velocimetry (PIV) allowed us to calculate velocity field and streamlines along the flow over bottom racks. Values are compared with numerical simulations. Figures 3-5 show the velocity vector field, together with the streamlines and the free surface flow profile are presented for approximation flow of q_1 = 77.0; 114.6 and 138.8 l/s/m, void ratio m = 0.28 and horizontal rack slope. Data consists in a steady state test. Free surface is measured in lab, with a good agreement with CFD numerical simulation (Castillo et al., 2014, 2016).Velocities and streamlines show a good agreement between measured and simulated values.

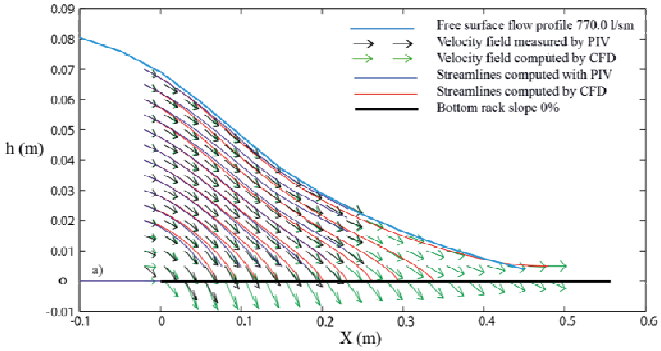

Figure 3. Velocity field and streamlines measured with PIV and simulated with CFD for rack with m = 0.28, horizontal slope and approximation flow, q_1 = 77.0 l/s/m.

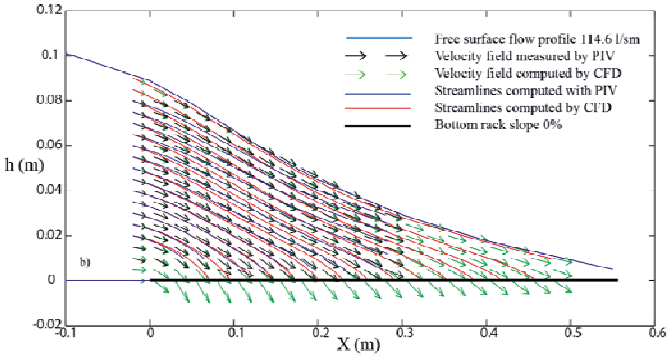

Figure 4. Velocity field and streamlines measured with PIV and simulated with CFD for rack with m = 0.28, horizontal slope and approximation flow, q_1 = 114.6 l/sm.

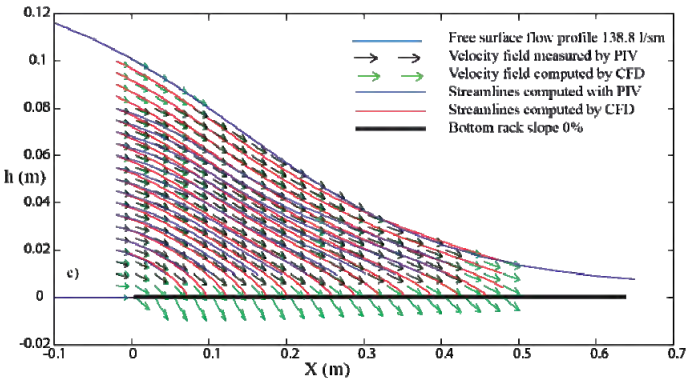

Figure 5. Velocity field and streamlines measured with PIV and simulated with CFD for rack with m = 0.28, horizontal slope and approximation flow, q_1 = 138.8 l/sm.

4.2 *Velocity and pressure coefficients*

The coefficients of velocity (α) and pressure (λ) of the energy equation can be obtained, by numerical integration, from the following equations:

$$\alpha = \frac{\int U_i^3 dA}{U^3 A} \quad (6)$$

$$\lambda = \frac{1}{qh}\int\left[\frac{p}{\gamma} + y\right]udA \tag{7}$$

where U_i is the horizontal component of the vector velocity, U the velocity module of the cross section, A the area of flow, q the specific flow across the considered section, y the vertical coordinate of the point in the cross section, and p the pressure in the point in which the y value is considered.

In Figures 6 and 7, the coefficients of velocity and pressure from equations 6 and 7 are shown for different cross sections located in different distances to the beginning of the rack (0.00, 0.05, 0.10, 0.20, and 0.30 m), as well as for three specific approximation flows (77.0, 114.6, and 138.8 l/s/m).

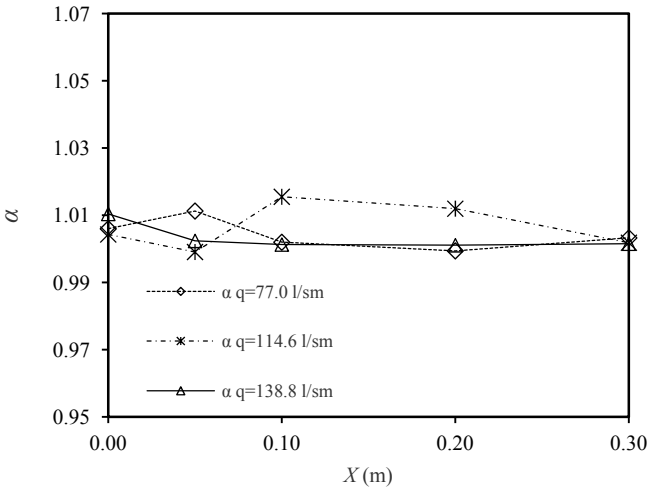

Figure 6. Velocity coefficient of the energy equation, α, in cross sections located X distances from the beginning of the rack, and for three specific approximation flows.

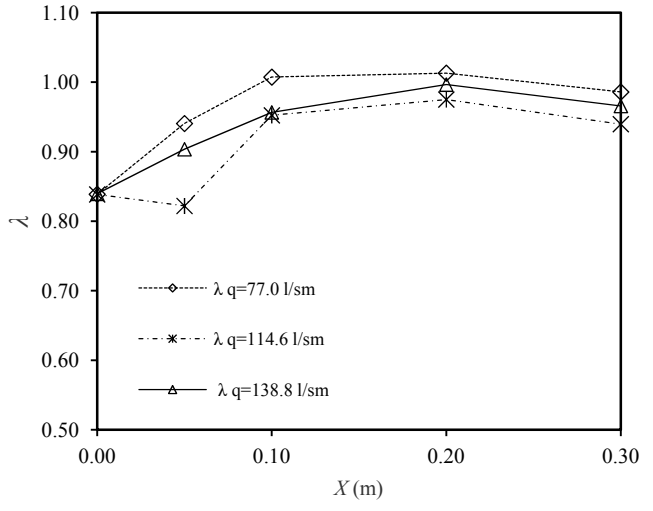

Figure 7. Pressure coefficient of the energy equation, λ, in cross sections located X distances from the beginning of the rack and for three specific approximation flows.

Coefficients presented in Figure 6 and 7 are obtained as a result of the proportional weight of the areas located over and between the longitudinal bars of the rack. From these coefficients, the Equation 2 can be numerically solved using the fourth-order Runge–Kutta algorithm. To solve the system, the equation of flow derived is required:

$$q' = \frac{dq}{dx} = -C_q m\sqrt{2gh} \tag{8}$$

The system of Equations 2 and 8 is equivalent to the solution of two ordinary differential equations with the unknown quantities $h(x)$ and $q(x)$.

At the inlet section, two boundary conditions are considered: the inlet specific flow q and the initial water depth h (being energy estimated as critical section).

Along the rack, the values of α, $d\alpha/dx$, λ, and $d\lambda/dx$ can be adjusted to exponential functions, expressed as functions of the x coordinate.

The discharge coefficient value is obtained from (Noseda, 1956):

$$C_q = \left[0.66m^{-0.16}\left(\frac{h}{l}\right)^{-0.13}\right] \tag{9}$$

where l is the interaxis distance. In this case, the interaxis distance is 0.0417 m.

The numerical results for $h(x)$ and for the derived flow q_d obtained are in agreement with the laboratory measurements. Figure 8 shows the results obtained for the specific flow of 114.6 l/s/m.

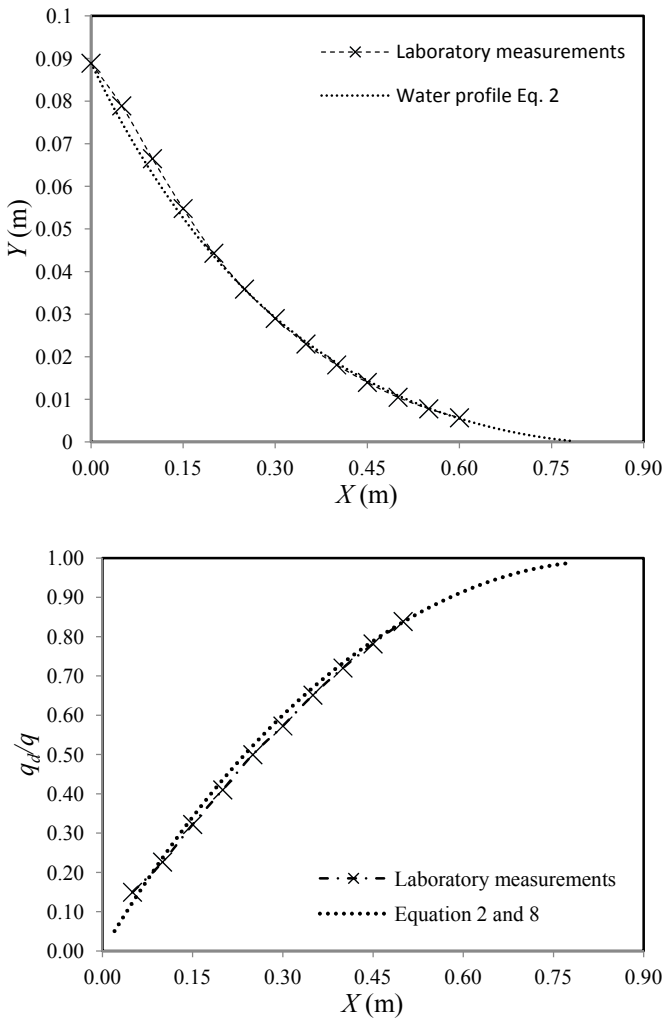

Figure 8. Comparison of the flow profile over the bottom rack and the flow derived along the rack solved with equations 2 and 8, and with laboratory measurements.

4.3 *Pressure head along the rack*

The curvature of streamlines in the flow leads to pressure deviations from hydrostatic conditions. Castro-Orgaz and Hager (2011) proposed an expression to calculate this deviation:

$$\Delta p = \frac{U^2}{2g}\left(hh'' - h'^2\right)\left(1-\frac{y^2}{h^2}\right) + \frac{U^2}{g}\left[-\left(\frac{q'h}{q}\right)^2\left(\frac{1}{2}-\frac{y}{h}+\frac{y^2}{2h^2}\right)\right] + \frac{U^2}{g}\left[\frac{q'hh'}{q}\left(\frac{5}{4}-\frac{3y}{2h}+\frac{y^2}{4h^2}\right)\right] \quad (10)$$

where Δp is the pressure deviation, g the gravitational acceleration, $q' = dq/dx$ the derived flow (Equation 8), $h' = dh/dx$ the slope of the surface of flow, and $h'' = d^2h/dx^2$ the curvature of flow profile.

From the field of velocities along the flow, in Figures 9-12 the three terms on the right side of Equation 10 are calculated and compared with the pressure head computed with CFD, p_{CFD}, in several cross sections and along the flow depth for the case of q=114.6 l/sm. Equation 11 shows the terms on the right side of Equation 10 defined as *Δp I, Δp II, Δp III and ΣΔp:*

$$\Delta pI = \frac{U^2}{2g}\left(hh'' - h'^2\right)\left(1-\frac{y^2}{h^2}\right)$$

$$\Delta pII = \frac{U^2}{g}\left[-\left(\frac{q'h}{q}\right)^2\left(\frac{1}{2}-\frac{y}{h}+\frac{y^2}{2h^2}\right)\right]$$

$$\Delta pIII = \frac{U^2}{g}\left[\frac{q'hh'}{q}\left(\frac{5}{4}-\frac{3y}{2h}+\frac{y^2}{4h^2}\right)\right]$$

$$\Sigma\Delta p = \Delta pI + \Delta pII + \Delta pIII \quad (11)$$

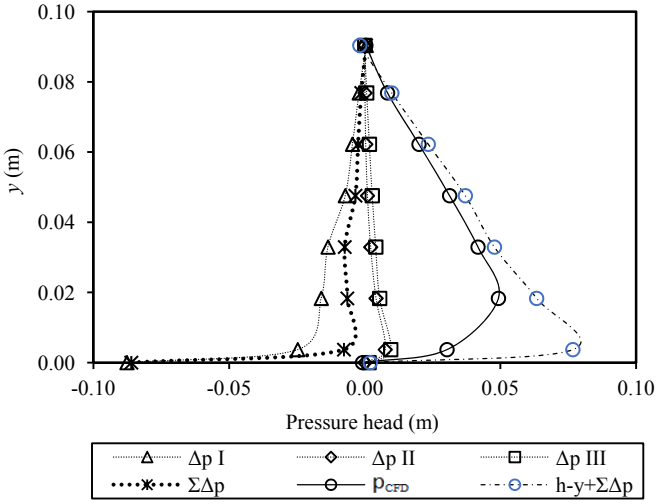

Figure 9. Pressure head calculated from velocity field and equation 10 compared with pressure head computed with CFD in a cross section located 0.00 m from the beginning of the rack.

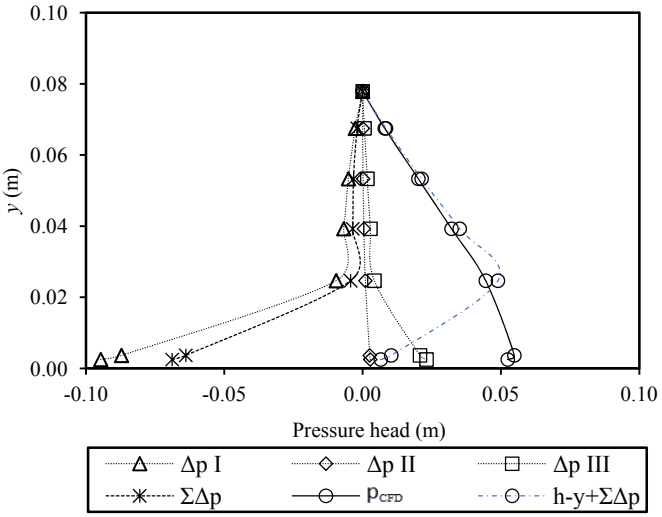

Figure 10. Pressure head calculated from velocity field and equation 10 compared with pressure head computed with CFD in a cross section located 0.05 m from the beginning of the rack.

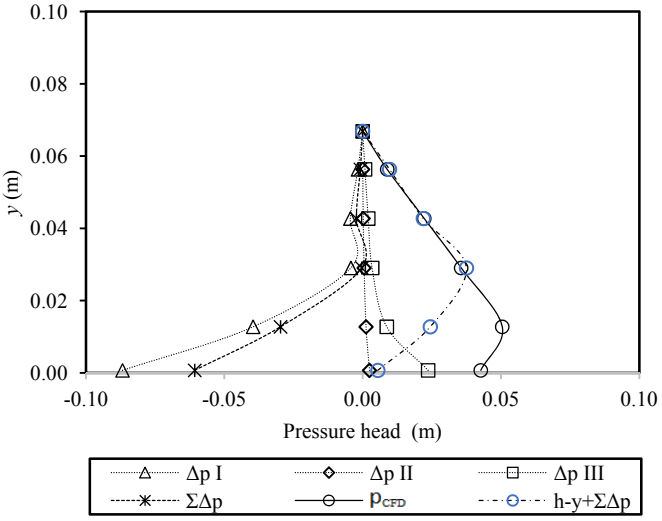

Figure 11. Pressure head calculated from velocity field and equation 10 compared with pressure head computed with CFD in a cross section located 0.10 m from the beginning of the rack.

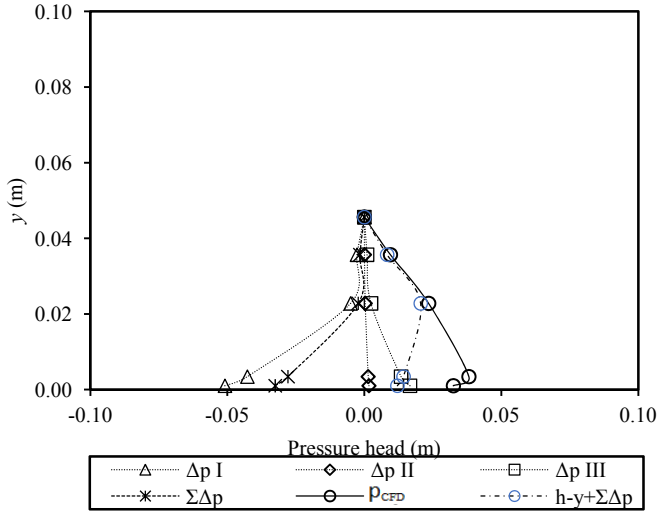

Figure 12. Pressure head calculated from velocity field and equation 10 compared with pressure head computed with CFD in a cross section located 0.20 m from the beginning of the rack.

Some differences are observed between the terms of pressure head computed with CFD, p_{CFD}, and the term (h-y+ $\Sigma\Delta p$) computed from velocity field and equation 10 (Castro-Orgaz and Hager, 2011). These differences are significant in the lower zones of the flow, near to the bottom rack, while 2-3 cm above the bottom rack, values are very similar.

From the Euler equation in the vertical direction and the continuity equation, the term Δp (Equation 10) was obtained by integration in the vertical direction.

The zones near the bottom rack are characterized with significant shear stress due to the increment of turbulence generated by a relevant transversal derivative of the vertical velocity within that area. Actually, vertical velocity has to change from significant values in the centre of the spacing between bars, to near null values close to the rack.

Thus as a first approximation, the term of viscous stresses that would appear in the vertical Euler equation, $\upsilon_t\left(\frac{\partial^2 U_y}{\partial x^2}+\frac{\partial^2 U_y}{\partial y^2}+\frac{\partial^2 U_y}{\partial z^2}\right)$, has been calculated, resulting in a new equation system:

$$\frac{1}{g}\left(U_x\frac{\partial U_y}{\partial x}+U_y\frac{\partial U_y}{\partial y}\right)=-\frac{1}{\rho g}\frac{\partial p}{\partial y}-\cos\theta+\frac{\upsilon_t}{g}\left(\frac{\partial^2 U_y}{\partial x^2}+\frac{\partial^2 U_y}{\partial y^2}+\frac{\partial^2 U_y}{\partial z^2}\right)$$
$$\frac{\partial U_x}{\partial x}+\frac{\partial U_y}{\partial y}=0 \qquad (12)$$

where U_x and U_y are the horizontal and vertical velocity components, respectively, and υ_t the kinematic eddy viscosity.

Neglecting terms of $\frac{\partial^2 U_y}{\partial x^2}+\frac{\partial^2 U_y}{\partial y^2}$, a numerical integration in the vertical direction has been done. Kinematic eddy viscosity divided by gravity acceleration is in the order of 10^{-4} ms, while the term $\frac{\partial^2 U_y}{\partial z^2}$ shows values in order of 10^3 $m^{-1}s^{-1}$. Integrating in the vertical direction, values of 10^{-2} m are obtained in the bottom part of the flow. These results are in agreement with the differences between p_{CFD} and the term (h-y+ $\Sigma\Delta p$) showed in Figures 9-12.

5 CONCLUSIONS

The definition of the velocity field through the bottom racks is of importance to evaluate the derivation capacity and clogging phenomena over intake systems. In this work, Particle Image Velocimetry (PIV) laboratory measurements and Computational Fluid dynamics simulations (CFD) have been used to obtain the velocity field.

The knowledge of the velocity and the pressure coefficients in the energy equation, allows to define the flow profile and the derivation flow with a good agreement to the values measured in laboratory.

In a first approximation, pressure heads computed with CFD, show differences with empirical methods proposed that does not take into account turbulent viscous stresses.

Further experimental measurements and CFD simulation are required to improve the knowledge in curvilinear flows with decreasing discharge in bottom intake systems.

ACKNOWLEDGMENTS

The authors are grateful for the financial support received from the Seneca Foundation of Región de Murcia (Spain) through the project “Optimización de los sistemas de captación de fondo para zonas semiáridas y caudales con alto contenido de sedimentos. Definición de los parámetros de diseño”. Reference: 19490/PI/14.

REFERENCES

ANSYS Inc. 2010. ANSYS CFX. Solver Theory Guide. Release 13.0.

Castillo, L. & Carrillo, J.M. 2012. Numerical simulation and validation of intake systems with CFD methodology. *Proc. 2nd IAHR European Congress; Munich, 27-29 June 2012.*

Castillo, L.G., Carrillo, J.M. & García, J.T. 2013a. Comparison of clear water flow and sediment flow through bottom racks using some lab measurements and CFD methodology. *Proc. Seven River Basin Management. Wessex Institute of Technology; New Forest, 22-24 May 2013.*

Castillo, L.G., Carrillo, J.M. & García, J.T. 2013b. Flow and sediment transport through bottom racks. CFD application and verification with experimental measurements. *Proc. 35th IAHR Congress, Chengdu, 8-13 September 2013.*

Castillo, L.G:, García, J.T., and Carrillo, J.M. 2014. Experimental measurements of flow and sediment transport through bottom racks. Influence of graves sizes on the rack, Proc. International Conference on Fluvial Hydraulics, 2014.

Castillo, L.G:, García, J.T., and Carrillo, J.M. 2015. Effective void ratio and rack length definition by experimental measurements of flow with gravel size sediments through bottom racks. E-proceedings of the 36th IAHR World Congress 28 June – 3 July, 2015, The Hague, the Netherlands.

Castillo, L.G:, García, J.T., and Carrillo, J.M. 2016. "Experimental and Numerical Study of Bottom Rack Occlusion by Flow with Gravel-Sized Sediment Application to Ephemeral Streams in Semi-Arid Regions". Water 2016, 8, 166; doi:10.3390/w8040166.

Castro-Orgaz, O., W. H. Hager. 2011. “Spatially-varied open channel flow equations with vertical inertia”. Journal of Hydraulic Research, 49:5, 667-675

De Marchi, G. 1947. “Profili longitudinali della superficie libera delle correnti permanenti lineari con portata progressivamente crescente o progressivamente decrescente entro canali di sezione costante”. Ricerca scientifica e ricostruzione.

Garot, F. 1939. De Watervang met liggend rooster, De Ingenieur in Nederlandsch Indie, 1939.

Mostkow, M. 1957. Sur le calcul des grilles de prise d'eau, La Houille Blanche, 4, 569-576, 1957.

Nakagawa, H. 1969. On Hydraulic performance of bottom diversión Works. Bulletin of Disaster Prevention Research Institute, Kyoto University.

Nasser, M. S., P. Venkataraman & A. S. Ramamurthy 1980. Flow in a channel with a slot in the bed, Journal of Hydraulic Research, 18:4, 359-367

Noseda, G. 1956. Correnti permanenti con portata progressivamente decrescente, defluenti su griglie di fondo, L'Energia Elettrica, 565-581, 1956.

Orth, J., Chardonnet, E. & Meynardi, G. 1954. Étude de grilles pour prises d'eau du type. La Houille Blanche 3: 343-351.

Righetti, M., and Lanzoni, S. 2008. Experimental Study of the Flow Field over Bottom Intake Racks. Journal of Hydraulic Engineering134(1): 15-22.

Thielicke, W. and Stamhuis, E. J. 2014. PIVlab - Time-Resolved Digital Particle Image Velocimetry Tool for MATLAB (version: 1.4). http://dx.doi.org/10.6084/m9.figshare.1092508